HHS Public Access

Author manuscript

Plast Reconstr Surg. Author manuscript; available in PMC 2020 January 01.

Published in final edited form as:

Plast Reconstr Surg. 2019 January ; 143(1): 77e–87e. doi:10.1097/PRS.0000000000005091.

Baseline lymphatic dysfunction amplifies the negative effects of lymphatic injury

Geoffrey E. Hespe, MD[#1], **Catherine L. Ly, MD**[#1], **Raghu P. Kataru, PhD**[1], and **Babak J. Mehrara, MD**[1]

[1]Plastic and Reconstructive Surgery Service, Department of Surgery, Memorial Sloan Kettering Cancer Center; New York, New York.

[#] These authors contributed equally to this work.

Abstract

Background: Genetic mutations and obesity increase the risk of secondary lymphedema, suggesting that impaired lymphatic function prior to surgical injury may contribute to disease pathophysiology. Previous studies show that obesity not only decreases lymphatic function, but also markedly increases pathologic changes, such as swelling, fibroadipose deposition, and inflammation. However, although these reports provide circumstantial evidence supporting the hypothesis that baseline lymphatic defects amplify the effect of lymphatic injury, the mechanisms regulating this association remain unknown.

Methods: Baseline lymphatic morphology, leakiness, pumping, immune cell trafficking, as well as local inflammation and fibroadipose deposition, were assessed in wild-type (WT) and Prox1-haploinsufficient ($Prox1^{+/-}$) mice, which have previously been showed to have abnormal vasculature without overt evidence of lymphedema. In subsequent experiments, WT and $Prox1^{+/-}$ mice underwent popliteal lymph node dissection (PLND) to evaluate the effect of lymphatic injury. Repeat testing of all variables was conducted four weeks post-operatively.

Results: At baseline, $Prox1^{+/-}$ mice had dilated, leaky lymphatic vessels corresponding to low-grade inflammation and decreased pumping and transport function, compared with wild-type (WT) mice. PLND resulted in evidence of lymphedema in both $Prox1^{+/-}$ and WT mice, but PLND-treated $Prox1^{+/-}$ mice had increased inflammation and decreased lymphatic pumping.

Conclusions: Subclinical lymphatic dysfunction exacerbates the pathologic changes of lymphatic injury, an effect that is multifactorial and related to increased lymphatic leakiness, perilymphatic accumulation of inflammatory cells, and impaired pumping and transport capacity. These findings suggest that pre-operative testing of lymphatic function may enable clinicians to more accurately risk-stratify patients and design targeted preventative strategies.

Corresponding Author: Babak J. Mehrara, MD; Member, Memorial Sloan Kettering Cancer Center; Professor of Surgery, Weill Cornell Medical College; 1275 York Avenue, Suite MRI 1006, New York, New York 10065; mehrarab@mskcc.org.

Author contributions

G.E.H, R.P.K., and B.J.M. conceived and designed the work; G.E.H. and R.P.K. conducted acquisition of data; G.E.H, C.L.L., R.P.K., and B.J.M. performed analysis and interpretation of data; and G.E.H, C.L.L., and B.J.M. drafted the work or revised it critically for important intellectual content.

Financial Disclosure Statement: None of the authors has a financial interest in any of the products, devices, or drugs mentioned in this manuscript.

Introduction

Lymphedema is a common complication of cancer treatment occurring in 30%–40% of patients who undergo lymph node dissection (1). Despite its prevalence, management remains limited due to the lack of an accurate risk stratification system and difficulties in prognosticating severity. Some are diagnosed after trivial lymphatic injury (i.e., sentinel lymph node biopsy), while others never develop the disease despite having known risk factors (2, 3). Similarly, certain patients display slow, smoldering disease in contrast to others with rapidly progressive disease regardless of treatment compliance. Elucidation of the mechanisms contributing to such variability is critical to improved care and is, therefore, an important research goal.

Recent studies have explored comorbidities that may increase the risk of lymphedema. Some, for example, have postulated that mutations in genes important in lymphatic regulation, such as hepatocyte growth factor, vascular endothelial growth factor 2 (VEGFR2), and VEGFR3 may predispose patients to the disease (4, 5). Similarly, others have found that high-fat diet-induced obesity (DIO) results in lymphatic impairment with decreased lymphatic endothelial cell (LEC) expression of lymphatic-related genes and that mice with DIO develop exaggerated deficits after injury (6–8). Such studies suggest that there may be a subset of patients in whom abnormal lymphatic development and/or dysregulation contribute to subclinical lymphatic dysfunction with a consequent elevated lymphedema risk. However, the means by which lymphatic abnormalities affect the development of lymphedema remain unclear. Elucidation of these pathways is critical, as it could allow for the implementation of preventative/therapeutic options in patients with such predisposition.

Because Prospero homeobox protein 1 (Prox1) is essential for LEC maintenance and migration (9, 10), mice that are heterozygous for the gene have subclinical lymphatic disease (11). Homozygous deletion results in embryonic lethality associated with severe edema secondary to the absence of lymphatic vessels, but haploinsufficient ($Prox1^{+/-}$) mice appear normal without overt evidence of edema (9, 12). Knowing this, we used popliteal lymph node dissection (PLND) to induce lymphatic injury in $Prox1^{+/-}$ mice to evaluate the effect of baseline lymphatic abnormalities on lymphedema pathogenesis.

Materials and Methods

Animals

All experiments were approved by the Institutional Animal Care and Use Committee at Memorial Sloan Kettering Cancer Center. Weight-matched (See Figure, Supplemental Digital Content 1, which shows the WT and $Prox1^{+/-}$ mice were weight-matched. Quantification of weight (grams) of WT and $Prox1^{+/-}$ mice at baseline [unpaired student's *t* test, mean (S.D.); n=4–5/group; P=0.41],) six-week-old male C57BL/6 mice (henceforth referred to as wild-type or WT mice) were purchased from Taconic Biosciences (Hudson, NY) and $Prox1^{+/-}$ mice were gifted by Dr. Guillermo Oliver (Northwestern University; Chicago, IL) (9). All mice were maintained in a light- and temperature-controlled environment. A minimum of four animals per group was utilized for each experiment. When

indicated, anesthesia was induced with isoflurane; tail pinch reflex and respiratory rate were monitored every 15 minutes to ensure adequate anesthesia. Euthanasia was conducted by carbon dioxide asphyxiation as recommended by the American Veterinary Medical Association.

Popliteal lymph node dissection (PLND)

We used a well-described model of PLND to study the effects of lymphatic injury on inflammation, lymphatic function, and lymphangiogenesis (13–15). After 30 μL of 3% Evans blue (Sigma-Aldrich; St. Louis, MO) in phosphate-buffered saline (PBS) was injected into the dorsal hindpaw to visualize the lymphatic system, the popliteal lymph node and its surrounding fat pad were excised, thereby removing both afferent and efferent vessels. The incision was closed with 3–0 continuous non-absorbable suture.

Analysis of lymphatic vessel morphology and leakiness

The ears of WT and Prox1$^{+/-}$ mice were injected with Evans blue or fluorescent tomato lectin to visualize the lymphatic vasculature (16, 17). In the apices of the right ears, we injected 2 μL of 1% Evans blue, which was allowed to disperse for 1 minute prior to imaging. Similarly, we injected 3 μL of 1 mg/mL tomato lectin (Sigma-Aldrich) in the apices of the left ears, followed by harvest 10 minutes later for whole-mount staining as described below.

Analysis of lymphatic function

Lymphoscintigraphy was used to assess baseline tail lymphatic transport capacity per published protocols (18, 19). Briefly, 50 μL of technetium-99m (^{99m}Tc; Nuclear Diagnostic Products; Rockaway, NJ) was injected intradermally 1 cm from the tail tip. An X-SPECT camera (Gamma Medica; Northridge, CA) was used to obtain images, and region-of-interest (ROI) analysis was accomplished using ASIPro Software (Siemans Medical Solutions USA; Knoxville, TN) to calculate decay-adjusted sacral lymph node uptake over 100 minutes.

We also performed microlymphangiography by injecting 2 mg/mL fluorescein isothiocyanate (FITC)-conjugated, lysine-flexible dextran (2000 kDA; Molecular Probes; Eugene, OR) into the distal tail (18). Images were obtained 15 minutes later at fixed 10-mm intervals using a SteREO Lumar V12 microscope (Zeiss; Munich, Germany) at fixed exposure, gain, and magnification.

Hindlimb lymphatic pumping and transport capacity were evaluated before and after PLND with near-infrared lymphangiography per previously reported techniques (20). A total of 15 μL of 0.15 mg/mL indocyanine green (ICG; Sigma-Aldrich) was injected intradermally into the dorsal hindpaw after hindlimb hair was removed with Nair depilatory cream (Church & Dwight Co.; Ewing, NJ). After 30 minutes of free ambulation, the mice were anesthetized and placed under a SteREO Lumar V12 microscope (Zeiss) with an EVOS EMCCD camera (Life Technologies; Carlsbad, California) and LED light source (CoolLED; Andover, UK) for 30 minutes. Collecting lymphatic vessel contractions per minute (packet frequency) was determined by changes in ICG intensity in a standard ROI over the dominant vessel after

subtracting background fluorescence using Fiji software (National Institutes of Health; Bethesda, MD).

Immune cell trafficking

Immune cell trafficking was assessed using FITC painting (21). Briefly, 40 μL of 8% 5 mg/mL FITC (Sigma-Aldrich) in a 1:1 mixture of acetone and dibutyl phthalate (Sigma-Aldrich) was painted onto hindpaws. Eighteen hours later, ipsilateral inguinal lymph nodes were harvested for flow cytometry as described below.

Immunohistochemistry

Immunofluorescent staining was performed per prior protocols (18). Tissues were fixed in 4% paraformaldehyde (PFA; Affymetrix; Cleveland, OH) prior to paraffin-embedding. Hindlimb tissues also underwent 2 weeks of decalcification with 0.5 M ethylenediaminetetraacetic acid (EDTA; Santa Cruz Biotechnology, Inc.; Dallas, TX). Blocks were cut into 5-μm sections, which were rehydrated before heat-mediated antigen retrieval using sodium citrate (Sigma-Aldrich) in a 90°C water bath. Sections were incubated overnight at 4°C with primary antibodies (Table 1) after non-specific binding was blocked with 20% donkey serum (Sigma-Aldrich) in PBS for 1 hour at room temperature. After washing, sections were incubated with fluorescent-labeled secondary conjugates (Life Technologies) for 5 hours then mounted with Mowiol (Sigma-Aldrich).

Mirax imaging software (Zeiss) with Imaris (Bitplane; Zurich, Switzerland) processing or a Leica SP5-U confocal microscope (Leica Microsystems, Inc.; Buffalo Grove, IL) with Zeiss Zen 2010 software was used for scanning. Cell counts were performed on high-powered sections by two blinded reviewers on a minimum of 4 mice per group and 4 high-powered sections per mouse using Pannoramic Viewer (3D Histech; Budapest, Hungary). Perilymphatic inflammation was assessed by quantifying cells within 50 μm of lymphatic vessels; the vessel with the greatest amount of inflammation was recorded for each high-powered field.

Flow cytometry

Flow cytometry was performed using previously described methods to assess dendritic cell (DC) migration (13). Single-cell suspensions were obtained through mechanical dissociation and enzymatic digestion with an 8:2:1 mixture of dispase II, collagenase D, and DNase I (Roche Diagnostics; Indianapolis, IN). Cells were stained with anti-CD11c (BioLegend; San Diego, CA) to identify DCs and 4,6-diamidino-2-phenylindole (DAPI; Molecular Probes) to exclude dead cells. A Fortessa flow cytometry analyzer (BD Biosciences; San Jose, CA) with BD FACSDiva software was used for data collection, and data were analyzed with FlowJo software (Tree Star; Ashland, OR).

Statistical analysis

Statistical analysis was performed using GraphPad Prism software (GraphPad Software, Inc., San Diego, CA). Unpaired student's paired *t* test and one-way analysis of variance (ANOVA) with the Brown-Forsythe test for group variance equality assessment and post-hoc Tukey's multiple comparisons test were used for comparing two and four groups,

respectively. Two-way ANOVA with post-hoc Sidak's multiple comparisons test was performed to analyze changes over time. Values are presented as mean and standard deviation unless otherwise noted, and $P<0.05$ was considered significant.

Results

Prox1-haploinsufficient mice have baseline lymphatic dysfunction

Studies have shown that Prox1$^{+/-}$ mice do not display the lymphedema phenotype despite having dilated, mispatterned lymphatic vessels (11, 12, 22). Consistent with this, Evans blue injection into the ears of Prox1$^{+/-}$ mice revealed aberrant lymphatic architecture with increased leakiness, as compared with WT mice (Fig. 1A). This was corroborated with immunofluorescent imaging with tomato lectin demonstrating dilated vessels with minimal lectin uptake, resulting in a stippled appearance of dye between vessels rather than intraluminal concentration as noted in controls (Fig. 1B).

The anomalous lymphatic morphology in Prox1$^{+/-}$ mice correlated with modestly but significantly diminished lymphatic transport capacity. Tail lymphoscintigraphy showed that Prox1$^{+/-}$ mice had a significant decrease in draining lymph node uptake compared to that in WT mice by 45 minutes post-injection (Fig. 1C; $P<0.05$ for indicated time points and $P=0.0066$ for peak uptake). Similarly, microlymphangiography demonstrated that Prox1$^{+/-}$ mice had increased pooling of dye due to dermal lymphatic vessel dilatation (See Figure, Supplemental Digital Content 2, which shows the Prox1$^{+/-}$ mice have impaired lymphatic transport function at baseline. Representative microlymphangiography images of mouse tails after injection of fluorescein isothiocyanate (FITC)-conjugated dextran into the distal tail). Collectively, such findings confirm that abnormal lymphatic vasculature in Prox1$^{+/-}$ mice is associated with global lymphatic leakiness and impaired transport function (12, 22).

Baseline lymphatic dysfunction results in increased inflammation following lymphatic injury

We then sought to evaluate how mice with baseline lymphatic dysfunction respond to lymphatic injury by performing PLND in both Prox1$^{+/-}$ and WT mice (Fig. 2A). Four weeks post-operatively, we assessed inflammation, diminished lymphatic vessel pumping, and dysfunctional lymphatic transport capacity, all of which are hallmarks of lymphedema.

At baseline, Prox1$^{+/-}$ mice had more perilymphatic accumulation of CD45^{+} leukocytes, as compared with WT mice, although this difference did not reach statistical significance (Fig. 2B; $P=0.15$) (See Figure, Supplemental Digital Content 3, which shows the Prox1$^{+/-}$ mice have amplified inflammatory responses following lymphatic injury. Representative immunofluorescent images co-localizing CD45^{+} cells (*upper*), CD4^{+} cells (*middle*), and F4/80^{+} macrophages with LYVE-1^{+} lymphatic vessels in ipsilateral hindlimb skin; scale bars, 50 μm,). As expected, PLND resulted in increased inflammation in both groups. However, the degree of inflammation in PLND-treated Prox1$^{+/-}$ mice was significantly more than that in their WT counterparts (Fig. 2B, Supplemental Digital Content 3 ***upper,*** ; $P=0.017$). Of note, the proportion of CD45^{+} cells in pre-PLND Prox1$^{+/-}$ mice was similar to that noted in post-PLND WT mice (Fig. 2B, Supplemental Digital Content 3 ***upper,*** ;

P>0.99). Interestingly, when we further characterized the $CD45^+$ cells, we found that there were significantly increased $CD4^+$ T cells (Fig. 2C ***left,*** Supplemental Digital Content 3 ***middle,*** ; P=0.048 and P=0.0075, respectively) and $F4/80^+$ macrophages (Fig. 2C ***right,*** Supplemental Digital Content 3 ***lower,*** ; P=0.019 and P=0.026, respectively) in $Prox1^{+/-}$ mice both before and after PLND, as compared with WT mice. Collectively, such data suggest that baseline lymphatic dysfunction is associated with mild subcutaneous inflammation, which is significantly amplified by lymphatic injury.

Baseline lymphatic dysfunction increases lymphatic leakiness and decreases pumping after PLND

Knowing that perilymphatic inflammation impairs collecting vessel pumping capacity by disrupting nitric oxide (NO) gradients (23, 24) and that pumping regulates as much as two-thirds of total lymphatic transport capacity (24), we then evaluated whether increased inflammation in $Prox1^{+/-}$ mice correlated with changes in lymphatic pumping. Using lymphangiography, we found that $Prox1^{+/-}$ mice had leakier lymphatic vessels manifesting as accumulation of dye in the skin (dermal backflow), as compared with WT controls at baseline (Fig. 3A ***left***). Similar to our ear studies (Fig. 1A-B), we also noted abnormal hypertrophic lymphatic vessels in the hindlimbs of pre-PLND $Prox1^{+/-}$ mice. These changes were markedly amplified after PLND (Fig. 3A ***right***). Although WT mice had a few areas of lymphatic leakiness, particularly around the surgical site, $Prox1^{+/-}$ mice had many more areas of leakiness, increased dermal backflow, and virtually no dye uptake. Pre-PLND $Prox1^{+/-}$ mice also had a 54% decrease in packet frequency as compared with WT mice, although this difference was not statistically significant (Fig. 3B ***upper***, 3C; P=0.090). Interestingly, however, the pumping in $Prox1^{+/-}$ mice was less regular than that in WT mice. After PLND, this disparity was markedly amplified, such that the PLND-treated $Prox1^{+/-}$ mice had a significant decrease in pumping (Fig. 3B ***lower***, 3C; P=0.039). While WT mice also had notably diminished packet frequency and changes in pumping regularity, there were hardly any contractions in post-PLND $Prox1^{+/-}$ mice and those that did occur were very irregular.

Changes in lymphatic pumping closely paralleled perilymphatic inducible nitric oxide synthase (iNOS) expression before and after surgery. At baseline, $Prox1^{+/-}$ mice had more perilymphatic $iNOS^+$ cells as compared with WT mice but this was not statistically significant (Fig. 3D; P=0.35**) (**See Figure, Supplemental Digital Content 4, which shows the $Prox1^{+/-}$ mice have attenuated lymphatic vessel pumping following lymphatic injury. Representative immunofluorescent images co-localizing $iNOS^+$ cells with $LYVE\text{-}1^+$ lymphatic vessels in ipsilateral hindlimb skin; scale bar, 50 μm,). PLND markedly increased the number of $iNOS^+$ cells in both groups with a significantly greater accumulation in $Prox1^{+/-}$ mice (Fig. 3D; P=0.0053) (Supplemental Digital Content 4,). Taken together, our findings suggest that baseline lymphatic defects increase capillary and collecting vessel leakiness and decrease collecting vessel pumping. This effect is highly amplified by lymphatic injury, resulting in worse impairment in interstitial fluid uptake by lymphatic vessels and more extensive dermal backflow. The impaired pumping may be, in part, due to perilymphatic accumulation of inflammatory cells expressing iNOS, which is known to

disrupt endogenous endothelial nitric oxide synthase (eNOS)-derived gradients of NO that regulate lymphatic pumping regularity and force.

Baseline lymphatic dysfunction exacerbates the effect of lymphatic injury on immune cell trafficking

In addition to being responsible for fluid homeostasis and macromolecule absorption, lymphatic vessels also play an essential role in immune cell trafficking (25). Knowing this, we hypothesized that Prox1 haploinsufficiency not only results in diminished lymphatic transport capacity in general, but also in impaired immune cell migration specifically. To evaluate this, we utilized FITC painting to assess DC migration from distal ipsilateral hindlimb tissues to inguinal lymph nodes, which are immediately upstream from the popliteal nodes (16), before and after PLND (Fig. 4A). In support of our hypothesis, at baseline, $Prox1^{+/-}$ mice had 82.6% fewer DCs in the lymph nodes as compared with controls (Fig. 4B; P=0.0032) (See Figure, Supplemental Digital Content 5, which shows the $Prox1^{+/-}$ mice have attenuated lymphatic transport capacity following lymphatic injury. FACS quantification of $CD11c^{-}FITC^{+}$ cells in ipsilateral inguinal lymph nodes after FITC painting onto distal mouse hindpaws [one-way ANOVA, mean (S.D.); n=4–5/group; 4 h.p.f./mouse, P=0.96 and P=0.048 for pre- and post-PLND, respectively]. Representative FACS plots of $CD11c^{+}FITC^{+}$ DCs in ipsilateral inguinal lymph nodes,). Because studies have shown that DC migration to nearby lymph nodes increase following injury (26), we suspected that PLND would lead to a greater accumulation of DCs in lymph nodes, especially because inguinal lymph nodes become the closest skin-draining nodes after popliteal lymphadenectomy. Consistent with this, there were significant more DCs in the nodes of PLND-treated WT mice compared to their pre-surgery counterparts (Fig. 4B, Supplemental Digital Content 5, INSERT LINK; P=0.021). In contrast, however, there was no notable difference in pre- and post-PLND $Prox1^{+/-}$ mice (Fig. 4B, Supplemental Digital Content 5, INSERT LINK; P=0.97). Such results provide further evidence that baseline lymphatic defects amplify lymphatic abnormalities post-operatively. Because lymphocytes also exit tissues via lymphatic vessels (27), this also suggests that increased leukocyte accumulation at baseline and following lymphatic injury results, at least in part, from impaired clearance of immune cell infiltration.

Discussion

Despite evidence that lymphedema is increasing in prevalence (28), management of this morbid disease is hindered by lack of knowledge regarding the factors influencing its variable natural history (29, 30). Some risk factors have been identified (2, 30, 31), but it remains difficult to predict whether an individual will develop lymphedema and, if he or she does, if he or she will have mild or severe manifestations. Guidelines based on risk factors have been useful to identify high-risk patients (28, 32), but, ultimately, the development of effective prophylactic regimens requires the understanding of the mechanisms underlying lymphedema pathogenesis in the setting of such risk factors.

Recent studies suggest that patients with breast cancer-related lymphedema (BRCL) may have had underlying lymphatic abnormalities that elevated their risk of developing the

disease. Cintolesi et al., for example, found that those who were ultimately diagnosed with BRCL had constitutively higher lymphatic pump pressures and transport function prior to cancer treatment (33). These authors suggested that these patients exhibited increased lymphatic work in response to chronically high preload and that they developed BCRL due to lower reserve pump capacity resulting in gradual lymphatic failure, analogous to that which occurs in hypertensive cardiac failure.

Baseline lymphatic dysfunction may be due to a variety of etiologies. Some have hereditary predisposition secondary to mutations in lymphatic-related genes (4, 5, 34). Obesity, however, is a common cause; it has been found to be an independent risk factor for lymphedema, possibly due to its negative effect on lymphatic function (35). Greene et. al, for example, found that patients with extreme obesity (body mass index >59 kg/m^2) spontaneously developed lymphedema (36). Using a mouse model of obesity, Weitman et al. showed that DIO contributed to impaired lymphatic transport function with corresponding changes in lymph node architecture (8). Further research revealed that such dysfunction corresponds to perilymphatic accumulation of inflammatory cells and lipids, in addition to decreased LEC expression of some of the same genes mutated in patients with genetic susceptibility to lymphedema (5, 6). Finally, by combining obesity and lymphedema models, Savetsky et al. demonstrated that mice with DIO have increased adipose deposition, inflammation, and reaction to noxious stimuli, compared with lean mice, both at baseline and after lymphatic injury (7).

In this study, we hypothesized that mice with underlying lymphatic abnormalities due to Prox1 haploinsufficiency would have an accentuated response to lymphatic injury similar to that seen in mice with DIO. $Prox1^{+/-}$ mice were utilized because, similar to patients with subclinical lymphatic dysfunction, these mice do not display the lymphedema phenotype, despite evidence of defective lymphatic vessels (9, 11, 22). Although these mice do develop adult-onset obesity (22), we used weight-matched controls, thus limiting the potential negative effects of weight gain.

Consistent with our hypothesis, we found that, compared with WT mice, $Prox1^{+/-}$ mice had greater perilymphatic inflammation, decreased lymphatic pumping, and diminished DC migration after lymphatic injury. Interestingly, pre-PLND $Prox1^{+/-}$ mice shared many of the characteristics observed in PLND-treated WT mice, even though they do not appear to have lymphedema. The mechanisms underlying these findings need to be further explored, but such results provide additional evidence that baseline lymphatic dysfunction may be important in the development of lymphedema. This is clinically significant, as it suggests that evaluation of baseline lymphatic function in select patients may allow for more accurate patient risk stratification. There is ongoing research seeking to identify the ideal test for lymphatic function in patients, but lymphoscintigraphy and ICG lymphangiography, similar to that performed in mice in this study, have been shown to be effective means of objective and noninvasive detection of early lymphatic disease (37). Magnetic resonance lymphangiography is also a promising diagnostic option, but is not yet widely available (38, 39). Ultimately, patients who are found to have pre-operative lymphatic dysfunction may then undergo therapeutic measures to increase lymphatic functional reserve prior to surgery and/or be considered for prophylactic options to prevent secondary lymphedema entirely.

Supplementary Material

Refer to Web version on PubMed Central for supplementary material.

Acknowledgements

The authors are grateful to Dr. Guillermo Oliver at Northwestern University for his gift of the Prox1-haploinsufficient mice. In addition, the authors would like to thank Navid Paknejad, Ning Fan, Mesruh Turkekul, Sho Fujisawa, and Yevgeniy Romin of the Molecular Cytology Core at Memorial Sloan Kettering Cancer Center for assistance with both histology and tissue imaging (Cancer Center Support Grant P30 CA008748) and Dagmar Schnau for her copy editing.

This work was supported by the NIH R01 HL111130 grant to B.J.M., the NIH T32 CA009501 grant to C.L.L., and the NIH/NCI P30 CA008748 (Cancer Center Support Grant) to Memorial Sloan Kettering Cancer Center.

Presented at: Northeastern Society of Plastic Surgeons (NESPS) 34th Annual Meeting, ewport, Rhode Island; September 9, 2017

References

1. Asdourian MS, Skolny MN, Brunelle C, Seward CE, Salama L, Taghian AG Precautions for breast cancer-related lymphoedema: risk from air travel, ipsilateral arm blood pressure measurements, skin puncture, extreme temperatures, and cellulitis. The Lancet Oncology 2016;17:e392–405. [PubMed: 27599144]
2. Tsai RJ, Dennis LK, Lynch CF, Snetselaar LG, Zamba GK, Scott-Conner C The risk of developing arm lymphedema among breast cancer survivors: a meta-analysis of treatment factors. Ann Surg Oncol 2009;16:1959–1972. [PubMed: 19365624]
3. McLaughlin SA, Wright MJ, Morris KT, et al. Prevalence of lymphedema in women with breast cancer 5 years after sentinel lymph node biopsy or axillary dissection: objective measurements. J Clin Oncol 2008;26:5213–5219. [PubMed: 18838709]
4. Finegold DN, Schacht V, Kimak MA, et al. HGF and MET mutations in primary and secondary lymphedema. Lymphat Res Biol 2008;6:65–68. [PubMed: 18564920]
5. Newman B, Lose F, Kedda MA, et al. Possible genetic predisposition to lymphedema after breast cancer. Lymphat Res Biol 2012;10:2–13. [PubMed: 22404826]
6. Garcia Nores GD, Cuzzone DA, Albano NJ, et al. Obesity but not high-fat diet impairs lymphatic function. Int J Obes (Lond) 2016;40:1582–1590. [PubMed: 27200507]
7. Savetsky IL, Torrisi JS, Cuzzone DA, et al. Obesity increases inflammation and impairs lymphatic function in a mouse model of lymphedema. American journal of physiology Heart and circulatory physiology 2014;307:H165–172. [PubMed: 24858842]
8. Weitman ES, Aschen SZ, Farias-Eisner G, et al. Obesity impairs lymphatic fluid transport and dendritic cell migration to lymph nodes. PloS one 2013;8:e70703. [PubMed: 23950984]
9. Wigle JT, Harvey N, Detmar M, et al. An essential role for Prox1 in the induction of the lymphatic endothelial cell phenotype. The EMBO journal 2002;21:1505–1513. [PubMed: 11927535]
10. Hong YK, Harvey N, Noh YH, et al. Prox1 is a master control gene in the program specifying lymphatic endothelial cell fate. Developmental dynamics : an official publication of the American Association of Anatomists 2002;225:351–357. [PubMed: 12412020]
11. Wigle JT, Oliver G Prox1 function is required for the development of the murine lymphatic system. Cell 1999;98:769–778. [PubMed: 10499794]
12. Harvey NL, Srinivasan RS, Dillard ME, et al. Lymphatic vascular defects promoted by Prox1 haploinsufficiency cause adult-onset obesity. Nat Genet 2005;37:1072–1081. [PubMed: 16170315]
13. Zampell JC, Yan A, Elhadad S, Avraham T, Weitman E, Mehrara BJ CD4(+) cells regulate fibrosis and lymphangiogenesis in response to lymphatic fluid stasis. PloS one 2012;7:e49940. [PubMed: 23185491]

14. Kwon S, Agollah GD, Wu G, Sevick-Muraca EM Spatio-temporal changes of lymphatic contractility and drainage patterns following lymphadenectomy in mice. PloS one 2014;9:e106034. [PubMed: 25170770]
15. Blum KS, Proulx ST, Luciani P, Leroux JC, Detmar M Dynamics of lymphatic regeneration and flow patterns after lymph node dissection. Breast Cancer Res Treat 2013;139:81–86. [PubMed: 23613202]
16. Harrell MI, Iritani BM, Ruddell A Lymph node mapping in the mouse. J Immunol Methods 2008;332:170–174. [PubMed: 18164026]
17. Tammela T, Saaristo A, Holopainen T, et al. Therapeutic differentiation and maturation of lymphatic vessels after lymph node dissection and transplantation. Nat Med 2007;13:1458–1466. [PubMed: 18059280]
18. Avraham T, Daluvoy S, Zampell J, et al. Blockade of transforming growth factor-beta1 accelerates lymphatic regeneration during wound repair. Am J Pathol 2010;177:3202–3214. [PubMed: 21056998]
19. Clavin NW, Avraham T, Fernandez J, et al. TGF-beta1 is a negative regulator of lymphatic regeneration during wound repair. American journal of physiology Heart and circulatory physiology 2008;295:H2113–2127. [PubMed: 18849330]
20. Zhou Q, Wood R, Schwarz EM, Wang YJ, Xing L Near-infrared lymphatic imaging demonstrates the dynamics of lymph flow and lymphangiogenesis during the acute versus chronic phases of arthritis in mice. Arthritis and rheumatism 2010;62:1881–1889. [PubMed: 20309866]
21. Randolph GJ, Angeli V, Swartz MA Dendritic-cell trafficking to lymph nodes through lymphatic vessels. Nat Rev Immunol 2005;5:617–628. [PubMed: 16056255]
22. Escobedo N, Proulx ST, Karaman S, et al. Restoration of lymphatic function rescues obesity in Prox1-haploinsufficient mice. JCI insight 2016;1.
23. Shirasawa Y, Ikomi F, Ohhashi T Physiological roles of endogenous nitric oxide in lymphatic pump activity of rat mesentery in vivo. American journal of physiology Gastrointestinal and liver physiology 2000;278:G551–556. [PubMed: 10762608]
24. Scallan JP, Zawieja SD, Castorena-Gonzalez JA, Davis MJ Lymphatic pumping: mechanics, mechanisms and malfunction. J Physiol 2016;594:5749–5768. [PubMed: 27219461]
25. Kim KW, Song JH Emerging Roles of Lymphatic Vasculature in Immunity. Immune network 2017;17:68–76. [PubMed: 28261022]
26. Lech M, Grobmayr R, Weidenbusch M, Anders HJ Tissues use resident dendritic cells and macrophages to maintain homeostasis and to regain homeostasis upon tissue injury: the immunoregulatory role of changing tissue environments. Mediators of inflammation 2012;2012:951390. [PubMed: 23251037]
27. Hunter MC, Teijeira A, Halin C T Cell Trafficking through Lymphatic Vessels. Frontiers in immunology 2016;7:613. [PubMed: 28066423]
28. Bevilacqua JL, Kattan MW, Changhong Y, et al. Nomograms for predicting the risk of arm lymphedema after axillary dissection in breast cancer. Ann Surg Oncol 2012;19:2580–2589. [PubMed: 22395997]
29. Tada H, Teramukai S, Fukushima M, Sasaki H Risk factors for lower limb lymphedema after lymph node dissection in patients with ovarian and uterine carcinoma. BMC cancer 2009;9:47. [PubMed: 19193243]
30. Kwan ML, Darbinian J, Schmitz KH, et al. Risk factors for lymphedema in a prospective breast cancer survivorship study: the Pathways Study. Arch Surg 2010;145:1055–1063. [PubMed: 21079093]
31. Warren AG, Brorson H, Borud LJ, Slavin SA Lymphedema: a comprehensive review. Ann Plast Surg 2007;59:464–472. [PubMed: 17901744]
32. Kuroda K, Yamamoto Y, Yanagisawa M, et al. Risk factors and a prediction model for lower limb lymphedema following lymphadenectomy in gynecologic cancer: a hospital-based retrospective cohort study. BMC women's health 2017;17:50. [PubMed: 28743274]
33. Cintolesi V, Stanton AW, Bains SK, et al. Constitutively Enhanced Lymphatic Pumping in the Upper Limbs of Women Who Later Develop Breast Cancer-Related Lymphedema. Lymphat Res Biol 2016;14:50–61. [PubMed: 27309032]

34. Finegold DN, Baty CJ, Knickelbein KZ, et al. Connexin 47 mutations increase risk for secondary lymphedema following breast cancer treatment. Clinical cancer research : an official journal of the American Association for Cancer Research 2012;18:2382–2390. [PubMed: 22351697]

35. Mehrara BJ, Greene AK Lymphedema and obesity: is there a link? Plast Reconstr Surg 2014;134:154e–160e.

36. Greene AK, Grant FD, Slavin SA, Maclellan RA Obesity-induced lymphedema: clinical and lymphoscintigraphic features. Plast Reconstr Surg 2015;135:1715–1719. [PubMed: 25724063]

37. Mihara M, Hara H, Narushima M, et al. Indocyanine green lymphography is superior to lymphoscintigraphy in imaging diagnosis of secondary lymphedema of the lower limbs. Journal of vascular surgery Venous and lymphatic disorders 2013;1:194–201. [PubMed: 26992343]

38. Arrive L, Derhy S, El Mouhadi S, Monnier-Cholley L, Menu Y, Becker C Noncontrast Magnetic Resonance Lymphography. J Reconstr Microsurg 2016;32:80–86. [PubMed: 25826439]

39. Borri M, Schmidt MA, Gordon KD, et al. Quantitative Contrast-Enhanced Magnetic Resonance Lymphangiography of the Upper Limbs in Breast Cancer Related Lymphedema: An Exploratory Study. Lymphat Res Biol 2015;13:100–106. [PubMed: 25774851]

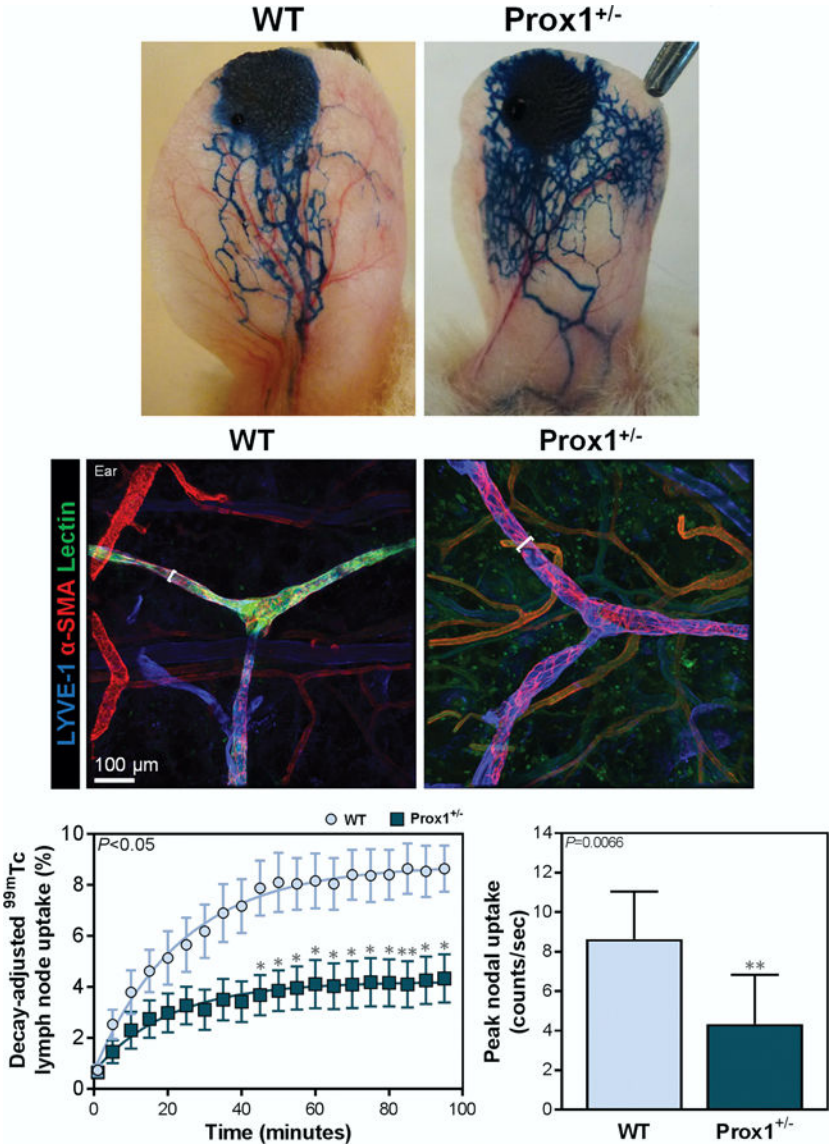

Figure 1. Prox1$^{+/-}$ mice have baseline lymphatic dysfunction.

A. Representative photographs of mouse ears after injection of Evans blue into anterior apices.

B. Representative immunofluorescent images of mouse ears co-localizing tomato lectin and LYVE^{+}α-SMA^{+} lymphatic vessels, with brackets indicating lymphatic vessel diameter; scale bar, 100 μm.

C. Quantification of decay-adjusted uptake [*left*; two-way ANOVA, mean (S.E.M.); n=8/group, P<0.05], and peak nodal uptake (*right*; unpaired student's *t* test, mean (S.D.); n=8/group; P=0.0066) of ^{99m}Tc by sacral lymph nodes after ^{99m}Tc injection into the distal tail.

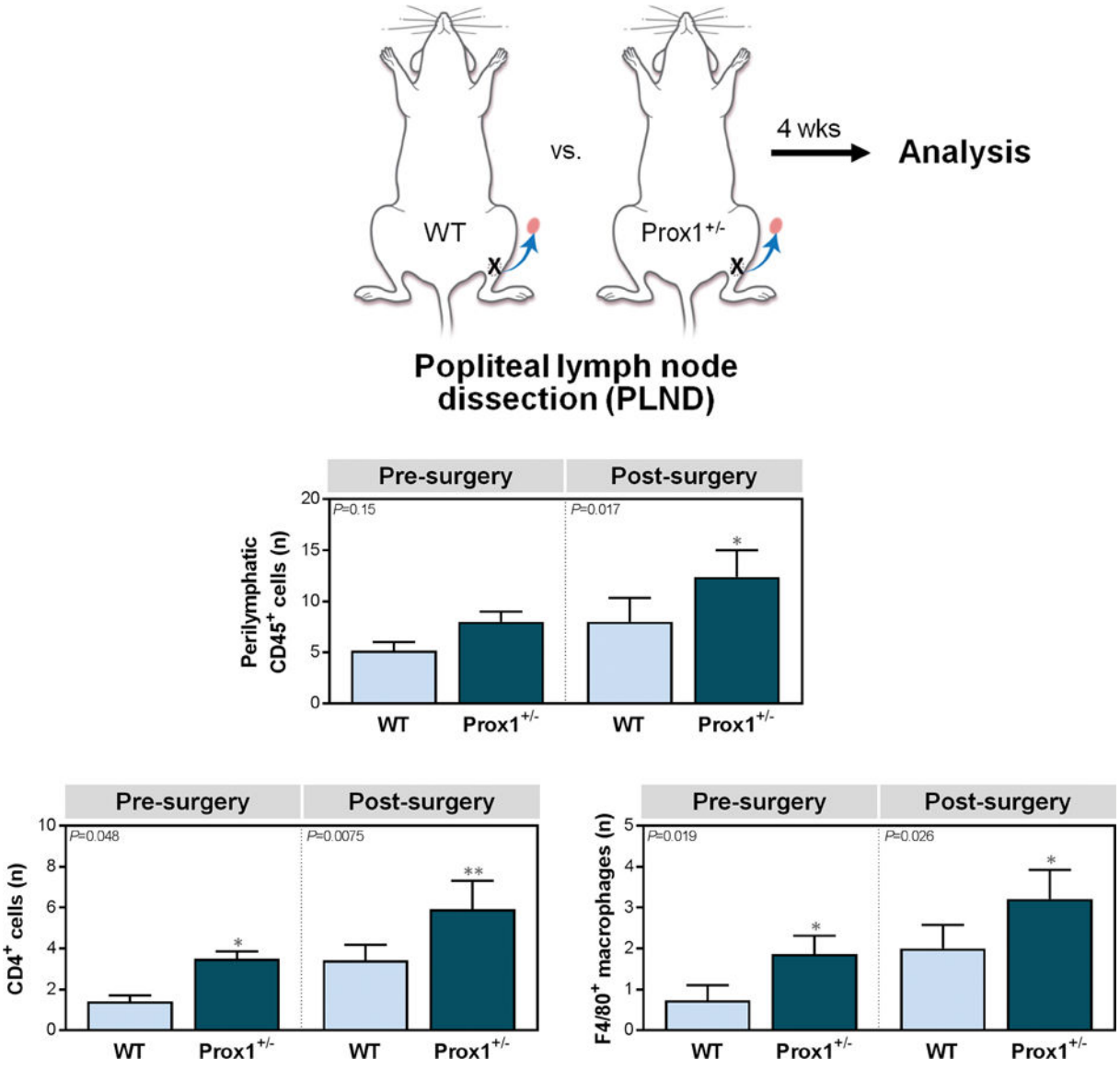

Figure 2. Prox1$^{+/-}$ mice have amplified inflammatory responses following lymphatic injury.

A. Schematic depiction of popliteal lymph node dissection (PLND).

B. Quantification of CD45^{+} cells within 50 μm of LYVE-1^{+} lymphatic vessels [one-way ANOVA, mean (S.D.); n=4–5/group; 4 high-powered fields (h.p.f.)/mouse, *P*=0.15 and *P*=0.017 for pre- and post-PLND, respectively].

C. Quantification of CD4^{+} cells [*left*; one-way ANOVA, mean (S.D.); n=4–5/group; 4 h.p.f./mouse, *P*=0.048 and *P*=0.0075 for pre- and post-surgery evaluation, respectively] and F4/80^{+} macrophages [*right*; one-way ANOVA, mean (S.D.); n=5/group; 4 h.p.f./mouse, *P*=0.019 and *P*=0.026 for pre- and post-PLND, respectively] within 50 μm of LYVE-1^{+} lymphatic vessels.

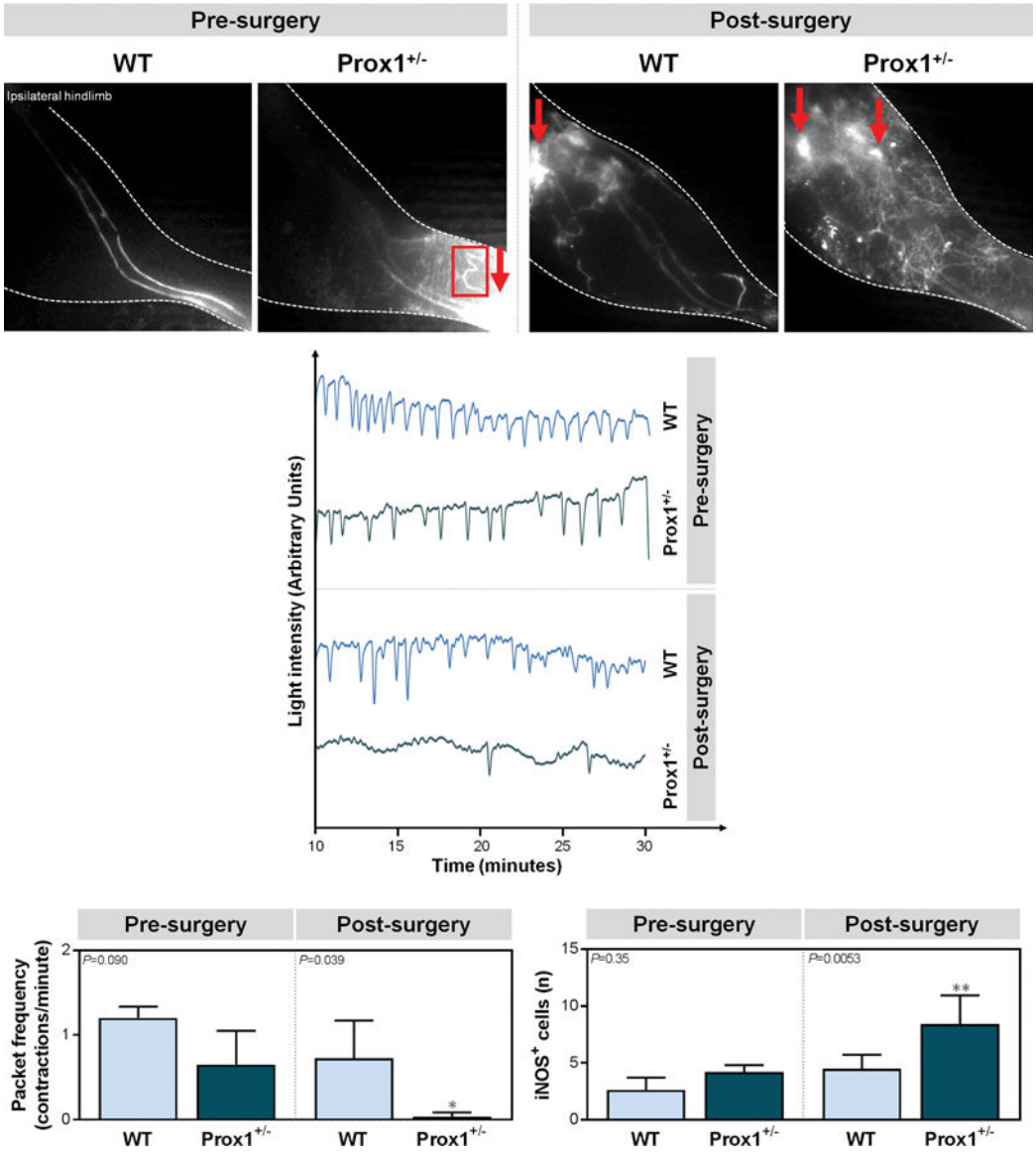

Figure 3. Prox1$^{+/-}$ mice have attenuated lymphatic vessel pumping following lymphatic injury.

A. Representative near-infrared lymphangiography images of ipsilateral mouse hindlimbs after indocyanine green (ICG) injection into the distal hindpaw, with red arrows representing dermal backflow and the red box indicating abnormal lymphatic vasculature.

B. Representative graphs of collecting lymphatic vessel pumping as determined by changes in ICG light intensity.

C. Quantification of packet frequency (lymphatic vessel contractions per minute) [one-way ANOVA, mean (S.D.); n=4–5/group; *P*=0.090 and *P*=0.039 for pre- and post-PLND, respectively].

D. Quantification of iNOS^{+} cells within 50 μm of LYVE-1^{+} lymphatic vessels [one-way ANOVA, mean (S.D.); n=5/group; 4 h.p.f./mouse, *P*=0.35 and *P*=0.0053 for pre- and post-PLND, respectively].

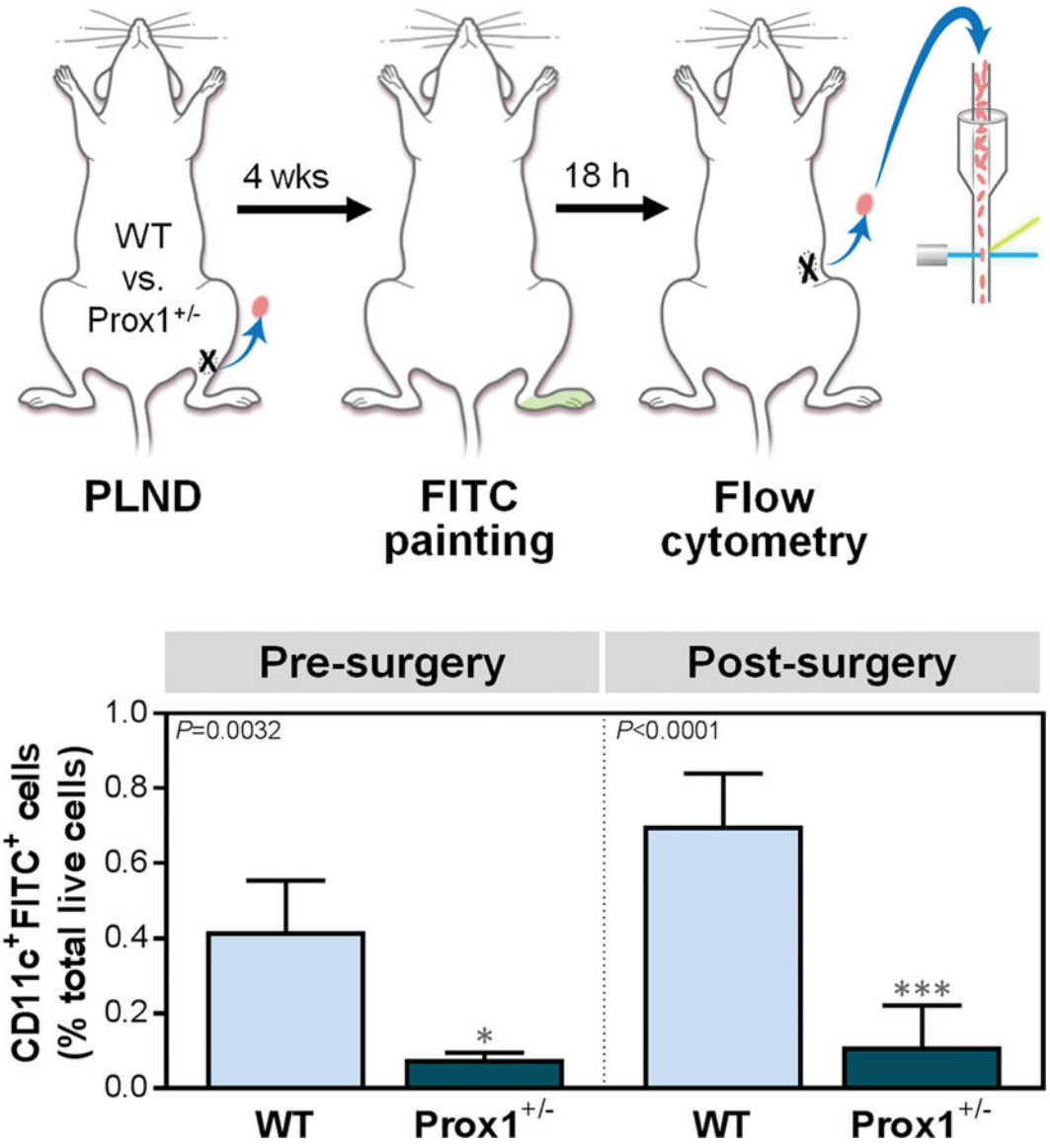

Figure 4. Prox1$^{+/-}$ mice have attenuated lymphatic transport capacity following lymphatic injury.

A. Schematic of experimental protocol for fluorescein isothiocyanate (FITC) painting.

B. FACS quantification of CD11c^{+}FITC^{+} dendritic cells (DCs) in ipsilateral inguinal lymph nodes after FITC painting onto distal mouse hindpaws [one-way ANOVA, mean (S.D.); n=4–5/group; 4 h.p.f./mouse, P=0.0032 and P<0.0001for pre- and post-PLND, respectively].

Table 1.

Primary antibodies for immunofluorescent staining.

Antigen	Type	Dilution	Manufacturer
Alpha-smooth muscle actin (α-SMA)	Mouse monoclonal	1:100	Sigma-Aldrich (St. Louis, MO)
CD4	Goat polyclonal	1:100	R&D Systems (Minneapolis, MN)
CD45	Rat monoclonal	1:100	R&D Systems
F4/80	Rat monoclonal	1:100	Abcam (Cambridge, MA)
Inducible nitric oxide synthase (iNOS)	Rabbit polyclonal	1:100	Abcam
LYVE-1	Goat polyclonal	1:400	R&D Systems